Facile Synthesis of Gold-Nanoparticle-Decorated $Gd_{0.3}Ce_{0.7}O_{1.9}$ Nanotubes with Enhanced Catalytic Activity for Oxygen Reduction Reaction

Chao Jin, Xuecheng Cao, Fanliang Lu, Zhenrong Yang, and Ruizhi Yang*

School of Energy & Collaborative Innovation Center of Suzhou Nano Science and Technology, Soochow University, Suzhou 215123, China

Ⓢ *Supporting Information*

ABSTRACT: We demonstrated a facile method to synthesize gold-nanoparticle-decorated $Gd_{0.3}Ce_{0.7}O_{1.9}$ (Au-GDC) nanotubes. X-ray diffraction, transmission electron microscopy, X-ray photoelectron microscopy, and energy-dispersive X-ray measurements were performed to characterize their structure and composition. In this unique structure, gold nanoparticles were uniformly decorated in the inner wall of $Gd_{0.3}Ce_{0.7}O_{1.9}$ (GDC) nanotubes with high gold loading. The catalytic activity of a Au-GDC nanotube catalyst for oxygen reduction reaction (ORR) in a 0.1 M KOH solution was studied using a rotating ring-disk electrode (RRDE) technique. RRDE results show that the ORR mainly favors a direct four-electron pathway, and a maximum cathodic limiting current density of -6.70 mA cm^{-2} at 2500 rpm was obtained, which is much bigger than that of gold bulk electrode and as-reported gold/rGO hybrid catalysts and close to the behavior of a commercial Pt/C catalyst below -0.8 V. Most importantly, the as-prepared Au-GDC nanotube catalyst exhibits excellent stability for the ORR because of the maximum interaction between gold nanoparticles and GDC nanotube supports.

KEYWORDS: *gold nanoparticle, $Gd_{0.3}Ce_{0.7}O_{1.9}$ nanotube, catalytic activity, oxygen reduction reaction*
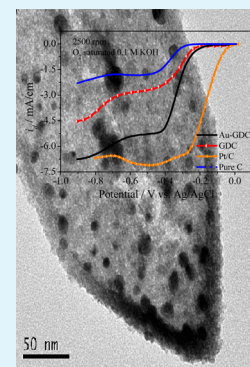
1. INTRODUCTION

The increasing energy demand of our society stimulates worldwide research activities for new energy conversion and storage systems. It is anticipated that electrochemical devices such as fuel cells and metal air batteries could be used for automotive applications in the future.[1,2] As one of the most important electrode reactions, oxygen reduction reaction (ORR) in the air electrode has been extensively studied in these fields.[3,4] It is well-known that platinum-based materials are the most active catalysts in state-of-the-art fuel cells, although the high cost and scarcity of platinum as well as the sluggish kinetics of the ORR stand in the way of their commercialization.[5-7] Therefore, developing highly efficient non-platinum catalysts for the ORR with comparable electrochemical performance has triggered extensive research interest.

Although experimental results and theoretical calculations have already proven that bulk gold (Au) has poor electrocatalytic activity for the ORR, recent studies have demonstrated that better electrocatalytic activity for the ORR could be obtained when we use Au nanoclusters as catalysts.[8-12] However, Au nanoclusters tend toward dissolution, aggregation, and sintering when they are used alone because of their extremely small size and high surface energy.[13,14] In order to overcome these obstacles, a feasible solution has been reported to fix Au nanoclusters on the specific supports with less or even without capping agents.[15,16] Among various possible support materials, metal oxide based on the bifunctional mechanism has been regarded as a promising one for the electronic effect, size

and shape of metal oxide nanocrystals, and support effect.[17-22] Cerium oxides (CeO$_2$) have attracted much attention for their high oxygen ion conductivities and low prices, as well as their good mechanical resistances and anticorrosion abilities in alkaline media.[23-25] Recently, some researchers have prepared and investigated Au-CeO$_2$ composite materials; for example, Carrettin et al.[26] used the deposition−precipitation method to coat Au nanoparticles on the surface of CeO$_2$ particles. However, there are very few works on the structural design of CeO$_2$-based catalysts to enhance catalytic activities. Therefore, it is necessary and meaningful to investigate the structural design of a Au-CeO$_2$ cocatalyst to enhance the synergistic effect and catalytic performance.

Among all of the available support materials, the hollow structure has been considered as one of the promising structures for catalyst supports because the hollow geometry provides a high specific surface area, favoring better dispersion of metal nanoparticles.[27-30] So far, various approaches have been developed to fabricate a hollow nanostructure, among which the template method is commonly used.[28,30-33] Ce(OH)CO$_3$ is a useful template because it can be easily removed by acid washing or calcination. Chen et al.[34] chose Ce(OH)CO$_3$ nanorods as the template and successfully fabricated three types of CeO$_2$ nanotubes through interfacial

Scheme 1. Schematic Illustration of the Au-GDC Nanotube Preparation Process
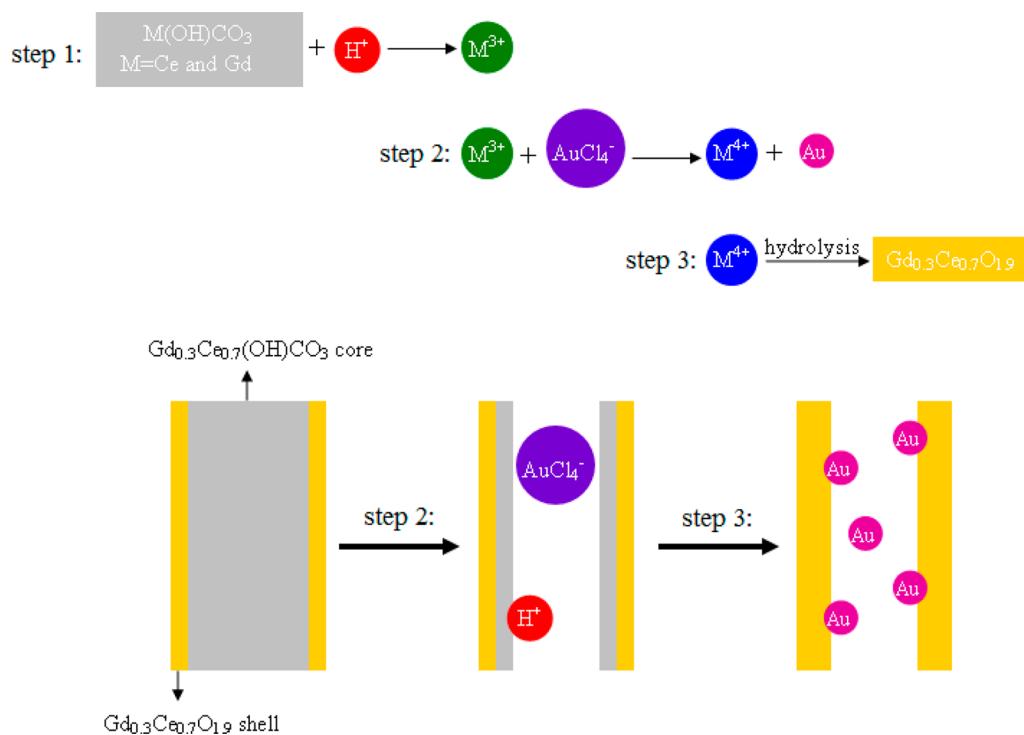
reactions. Furthermore, considering the reduction ability of cerium(III), these highly interesting $Ce(OH)CO_3$ nanorod templates may be further employed in oxidation−reduction reactions with oxidizing agents to form nanocomposite structures. In alkaline media, cerium(III) can be easily oxidized to cerium(IV) by oxygen, and cerium(IV) is inclined to be hydrolyzed to CeO_2, which is expected to deposit in situ on the residual $Ce(OH)CO_3$ surface to form a core−shell structure with $Ce(OH)CO_3$ as the core and CeO_2 as the shell. It is worth remembering that $HAuCl_4$ is a strong acid with strong oxidation owing to $AuCl^-$. So, it is entirely possible to get a Au-nanoparticle-decorated CeO_2 nanotube with $Ce(OH)CO_3$ as the template.

Gadolinium-substituted CeO_2, $Gd_{0.3}Ce_{0.7}O_{1.9}$ (GDC), has a higher oxygen storage capacity than pure CeO_2, which is widely used as a solid oxide fuel cell electrolyte material.[35,36] Herein, Au-nanoparticle-decorated GDC (Au-GDC) nanotubes have been successfully prepared through an in situ redox reaction between $HAuCl_4$ and a $Gd_{0.3}Ce_{0.7}(OH)CO_3$ nanorod template. Neither additional reducing agents nor stabilizing molecules are employed during the overall procedure. The electrochemical measurements show that significantly enhanced catalytic activity and stability for the ORR have been achieved.

2. EXPERIMENTAL DETAILS

Chemicals. The following analytical-grade chemicals were used as received: $Ce(NO_3)_3 \cdot 6H_2O$, $Gd(NO_3)_3 \cdot 6H_2O$, $HAuCl_4$, NaOH, and urea were purchased from Guoyao Chemical Reagent Co. Ltd. Nafion 117 solution (6% in ethanol), acetylene black, and a commercial 20 wt % Pt/C catalyst were purchased from Sigma-Aldrich.

Preparation of a $Gd_{0.3}Ce_{0.7}(OH)CO_3$ Nanorod Template. Stoichiometric $Ce(NO_3)_3 \cdot 6H_2O$ and $Gd(NO_3)_3 \cdot 6H_2O$ (total 0.004 mol) and urea (0.024 mol) were added to 80 mL of water in a sealed beaker under vigorous magnetic stirring at 80 °C for 24 h. The as-obtained powder sample was centrifuged, washed with distilled water, and dried at 60 °C for 12 h.

Preparation of a $Gd_{0.3}Ce_{0.7}(OH)CO_3$−$Gd_{0.3}Ce_{0.7}O_{1.9}$ (GDC) Core−Shell Structure. NaOH (0.06 mol) was added to 20 mL of water, and then the as-prepared $Gd_{0.3}Ce_{0.7}(OH)CO_3$ powder (0.087 g) was soaked in this NaOH solution for 72 h. The as-prepared light-yellow powder was centrifuged, washed with distilled water, and dried at 60 °C for 12 h.

Preparation of Au-Nanoparticle-Decorated $Gd_{0.3}Ce_{0.7}O_{1.9}$ (Au-GDC) Nanotubes. The as-prepared $Gd_{0.3}Ce_{0.7}(OH)CO_3$−GDC core−shell structure powder was added to 6 mL of $HAuCl_4$ (0.024 M) with slow stirring for 0.5 h, the mixture was kept at room temperature for 24 h, then centrifuged, and washed with distilled water and ethanol several times, and the as-obtained sample was dried at 180 °C for 12 h to obtain a purple target product.

Characterizations. The morphology and structure of the samples were characterized by high-resolution transmission electron microscopy (HRTEM; TecnaiG220) and X-ray diffraction (XRD; Bede Scientific Ltd.; Cu Kα radiation). Components of the samples were analyzed by X-ray photoelectron spectroscopy (XPS; VG ESCALAB MKII) and energy-dispersive X-ray spectrometry (EDX; Horiba EMAX 7539-H).

Electrochemical Measurements. As in our previously reported work,[37] the electrocatalytic activity for the ORR was studied with the rotating ring-disk electrode (RRDE) technique using a Pine electrochemical system (AFMSRX rotator and AFCBP1 bipotentiostat). The RRDE consisted of a catalyst film-coated glassy carbon (GC) disk (0.196 cm^2 of geometric surface area) surrounded by a platinum ring (0.125 cm^2 of geometric surface area). A conventional three-electrode single-compartment Pyrex glass cell was used to carry out electrochemical investigations at room temperature. A platinum wire was used as the counter electrode, and an Ag/AgCl (1 M Cl^-, 0.20 V vs NHE) reference electrode was used in a double-junction reference chamber. All potential values mentioned in the text are given against this reference only. The electrolyte was a 0.1 M KOH solution prepared with ultrapure water (Millipore, 18.2 MΩ cm).

The catalyst ink of the dispersed Au-GDC nanotube was made by mixing 5 mg of Au-GDC nanotube powder and 5 mg of acetylene black with 95 µL of Nafion solution and 350 µL of ethanol in an ultrasonic bath for 2 h. The working electrode was prepared by applying 7 µL of catalyst ink to the surface of the GC electrode with a
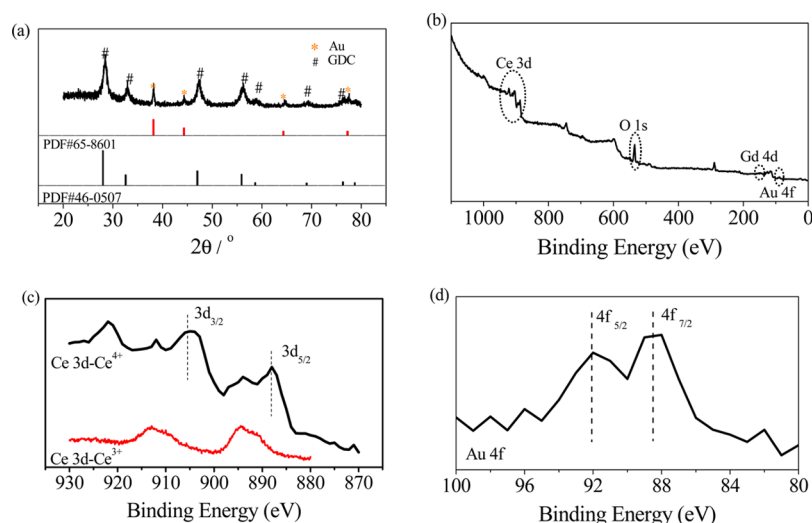
Figure 1. (a) XRD pattern of the as-prepared Au-GDC nanotube. (b) Full XPS spectra of the as-prepared Au-GDC nanotube. (c) XPS spectra of Ce 3d of the as-prepared Au-GDC nanotube (black line) and $Gd_{0.3}Ce_{0.7}(OH)CO_3$ precursor (red line). (d) XPS spectra of Au 4f of the as-prepared Au-GDC nanotube.

micropipet and drying in air for 0.5 h. The catalyst loading was 0.4013 mg cm^{-2}.

RRDE voltammetric experiments were performed for the ORR test with a 10 mV s^{-1} scanning rate in an O_2-saturated 0.1 M KOH solution at room temperature. The voltage scanning range was from −1.0 to 0.2 V. The ring potential was set at 0.5 V, which is considered to be sufficiently high to induce complete peroxide decomposition as reported elsewhere.[38] During the ORR test, the background capacitive current contribution (obtained from a N_2-saturated experiment) is subtracted from each voltammogram. Prior to each measurement, the KOH solution was bubbled with either N_2 or O_2 at a flow rate of 25 sccm over 0.5 h for the ORR.

3. RESULTS AND DISCUSSION

Synthesis and Characterization of Au-GDC Nanotubes. In this work, a $Gd_{0.3}Ce_{0.7}(OH)CO_3$ nanorod was first prepared as the precursor, the XRD and TEM analysis of which are shown in Figure S1 in the Supporting Information (SI); then the $Gd_{0.3}Ce_{0.7}(OH)CO_3$ precursor was immersed in a 3 M NaOH solution for 3 days to obtain a $Gd_{0.3}Ce_{0.7}(OH)CO_3$– GDC core−shell structure (see the TEM images shown in Figure S2 in the SI). On the basis of the $Gd_{0.3}Ce_{0.7}(OH)CO_3$– GDC core−shell precursor, a Au-GDC nanotube was finally obtained. Scheme 1 shows an illustration for the preparation of the Au-GDC nanotube catalyst. First, the $Gd_{0.3}Ce_{0.7}(OH)$- CO_3–GDC core−shell structure was immersed in a 0.024 M $HAuCl_4$ solution for 24 h. In the process of immersion, H$^+$ would react with the $Gd_{0.3}Ce_{0.7}(OH)CO_3$ core to dissolve it and release Gd^{3+} and Ce^{3+} ions, resulting in a hollow structure, and the $AuCl_4^-$ ion would simultaneously migrate to the interior of the GDC shell owing to the electrostatic attraction between H$^+$ and $AuCl_4^-$. Because Gd^{3+} and Ce^{3+} have certain reducing abilities, Au, Gd^{4+}, and Ce^{4+} ions would be achieved because of a redox reaction between $AuCl_4^-$ and the Gd^{3+} and Ce^{3+} ions. During the process of drying, Gd^{4+} and Ce^{4+} ions would hydrolyze to yield GDC, and an Au-GDC nanotube catalyst was finally obtained.

XRD analysis of the as-prepared Au-GDC nanotube catalyst was conducted, as shown in Figure 1a; the diffraction peaks of GDC and Au are observed as compared with standard PDF cards of GDC and Au. The Au nanoparticles have an average size of about 7 nm according to the Debye−Scherrer equation

calculation.[39] To obtain more detailed information about the elemental makeup and the oxidation state of the as-prepared Au-GDC nanotube, XPS measurements were performed, and the results are shown in Figure 1b−d. As shown in Figure 1c, the Ce 3d electron core level is characterized by two series of peaks: $3d_{5/2}$ and $3d_{3/2}$. Two characteristic peaks at 906 and 888 eV are ascribed to cerium(IV). For comparison, cerium(III) characteristic signals existing in the $Gd_{0.3}Ce_{0.7}(OH)CO_3$ precursor were also measured (red line in Figure 1c). The valence state of cerium increased from 3+ in the $Gd_{0.3}Ce_{0.7}(OH)CO_3$ precursor to 4+ in the as-prepared Au-GDC nanotube, suggesting the formation of GDC. Moreover, the binding energy of Ce 3d increases not only in the as-prepared Au-GDC nanotube but also in the $Gd_{0.3}Ce_{0.7}(OH)$- CO_3 precursor as compared with standard cerium(IV) and cerium(III) binding energies, suggesting that gadolinium substitution increased the binding energy of Ce 3d. In the case of the Au 4f core level spectrum (Figure 1d), the Au 4f peaks show a doublet at 92 and 88.5 eV corresponding to Au $4f_{5/2}$ and Au $4f_{7/2}$, respectively, suggesting that Au is mainly present in the Au^0 state. Also, the binding energy of Au 4f increases in the as-prepared Au-GDC nanotube, compared with the standard Au binding energy (87.6 and 83.6 eV), implying that a strong interaction exists between the Au nanoparticles and the GDC nanotube. From the XPS results, it can be clearly seen that an oxidation−reduction reaction indeed occurs between the $HAuCl_4$ and $Gd_{0.3}Ce_{0.7}(OH)CO_3$ nanorods.

The structure of the as-prepared Au-GDC nanotube was investigated by TEM. Figure 2 illustrates the morphology of the as-prepared sample. As observed from Figure 2a, well-dispersed Au nanoparticles were decorated in the inner wall of the GDC nanotube. The nanotube has a wall thickness of about 25 nm and a length of 1.5−2.0 um, while the size distribution of the Au nanoparticle is narrow with an average diameter of 7.5 nm (shown as the inset in Figure 2a). Detailed structure information of the as-prepared Au-GDC nanotube was further revealed using HRTEM. As shown in Figure 2b, the measured d spacing of 0.24 nm in the center of the particle is assigned to the lattice spacing of the (111) plane of Au. The interlayer distance of 0.32 nm in the outer region can be indexed to the lattice spacing of the (111) plane of GDC. Figure 2c exhibits

(a)

(b)

(c)
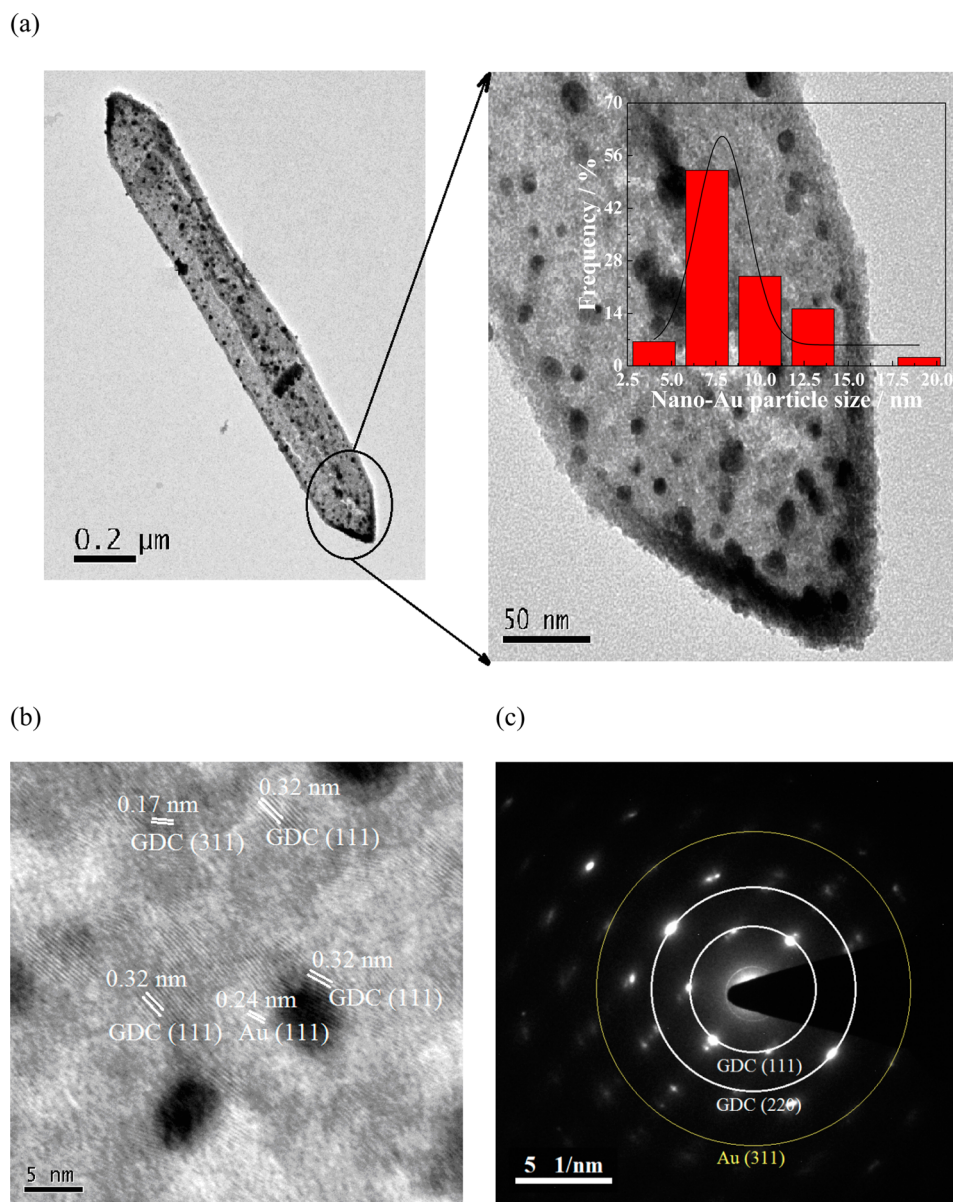
Figure 2. (a) TEM images of Au-GDC nanotubes with different magnifications. The inset shows the Au nanoparticle size distribution. (b) HRTEM image of the Au-GDC nanotube. (c) SAED patterns of the Au-GDC nanotube.

the selected-area electron diffraction (SAED) patterns of the Au-GDC nanotube. Two rings can be assigned to diffraction planes of the GDC shell, while the blurry scattered dots (marked with yellow ring) indicate that the Au nanoparticle bears a single-crystalline structure. To further study the local composition of the as-prepared Au-GDC nanotubes, TEM–EDX was examined, and the results are displayed in Figure S3 in the SI. An average atomic ratio of Au/M (M = Ce and Gd) of 0.3086 was obtained, suggesting a high loading of Au nanoparticles in the as-prepared Au-GDC nanotubes.

Catalytic Activity of the Au-GDC Nanotube for the ORR. Cyclic voltammetry (CV) scanning was performed to evaluate the ORR electrocatalytic activity of the as-prepared Au-GDC nanotube catalyst in an O_2- or a N_2-saturated 0.1 M KOH solution at room temperature, respectively, and these results are shown in Figure S4 in the SI. The comparison of the two CV curves in Figure S4 in the SI clearly shows the exceptional ORR catalytic activity of the as-prepared Au-GDC

nanotubes. The ORR onset potential is at ca. −0.14 V (vs Ag/AgCl) with two reduction peaks at ca. −0.33 and −0.76 V (vs Ag/AgCl), respectively. We then evaluated the electrocatalytic performance of the as-prepared Au-GDC nanotube catalyst for the ORR in an O_2-saturated 0.1 M KOH solution using a rotating disk electrode (RDE) at room temperature with a sweep rate of 10 mV s^{-1}. Figure 3 shows the ORR polarization curves at 2500 rpm for the as-prepared Au-GDC nanotubes, the pure carbon, the GDC nanoparticle, and the commercial 20 wt % Pt/C (platinum loading was 0.1605 mg cm^{-2}). As seen from Figure 3, the diffusion-limiting current density of the as-prepared Au-GDC nanotube is −6.50 mA cm^{-2} at −0.8 V, which is much bigger than that of the as-reported Au/rGO hybrid catalyst[16] (−4.70 mA cm^{-2} about at −0.8 V in 0.1 M KOH with a scanning rate of 50 mV s^{-1}) and close to that of the commercial Pt/C catalyst below −0.8 V, although the onset potential for the ORR is lower than that for Pt/C. Furthermore, the onset potential and diffusion-limiting current density for the
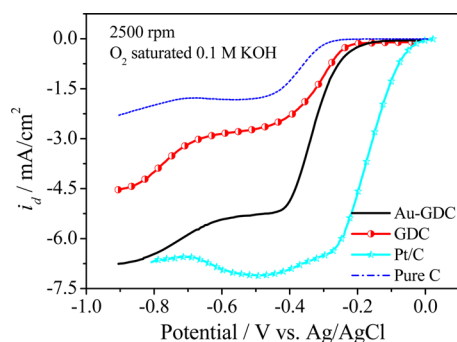
Figure 3. RDE curves of the as-prepared Au-GDC nanotubes, the pure carbon, the GDC nanoparticle, the Au bulk electrode, the commercial Pt/C, and the as-reported Au/rGO hybrid catalyst recorded in an O_2-saturated 0.1 M KOH solution at 2500 rpm.

ORR of the as-prepared Au-GDC nanotube are more positive and larger than that of the pure carbon and the GDC nanoparticle. Considering the Au loading of 0.1031 mg cm^{-2} calculated by the TEM−EDX test, these results suggest that the as-prepared Au-GDC nanotube is a promising catalyst for the ORR.

The as-prepared Au-GDC nanotube catalyst was further studied through the RRDE technique to evaluate the oxygen reduction kinetic parameters. The measurements were carried out in a cathodic sweep with 10 mV s^{-1} at various rotation speeds (ω) from 400 to 2500 rpm. Figure 4 shows both the
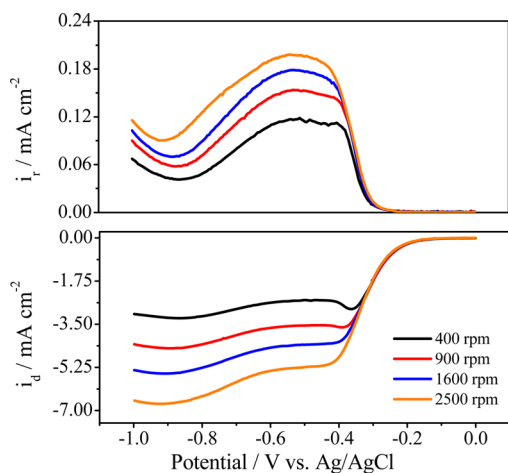
Figure 4. Disk current density (i_d) and ring current density (i_r) collected on the as-prepared Au-GDC catalyst during the ORR in an O_2-saturated 0.1 M KOH solution.

ring current density (i_r) and disk current density (i_d) of the as-prepared Au-GDC nanotube catalyst recorded in an O_2-saturated 0.1 M KOH solution. The RRDE experiment involves holding the disk at potential E_d, where the reaction $O + ne \rightarrow R$ produces a cathodic current i_d; the ring is kept at a sufficiently positive potential E_r (0.5 V), so that any R reaching the ring is rapidly oxidized.[40] The ring current, i_r, is related to the disk current, i_d, by a quantity N, the capture coefficient. So, the transferred electron number (n) and the contents of peroxide HO_2^- during the ORR could be calculated, according to eqs 1 and 2,[41] respectively, as follows:

$$n = 4\frac{i_d}{i_d + i_r/N} \tag{1}$$

$$HO_2^- \% = 100 \times \frac{2i_r/N}{i_d + i_r/N} \tag{2}$$

where n is the electron number transferred during the reaction, i_d is the disk current, i_r is the ring current, and N is the capture coefficient (here, $N = 0.22$).

The transferred electron number and contents of peroxide HO_2^- during the ORR are calculated and displayed in Figure 5.
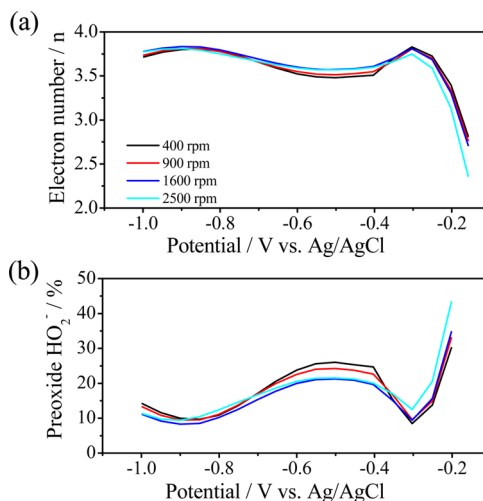
Figure 5. (a) Transferred electron number and (b) contents of peroxide HO_2^- during the ORR, which are calculated with i_d and i_r.

The n values are 3.5−3.8 over the potential range from −0.3 to −1.0 V (vs Ag/AgCl), suggesting that the as-prepared Au-GDC nanotube catalyst most likely favors the four-electron-reduction reaction process.

The ORR mechanism was further examined using the Koutecky−Levich (K−L) correlations. The K−L plots corresponding to the experimental disk current curves of
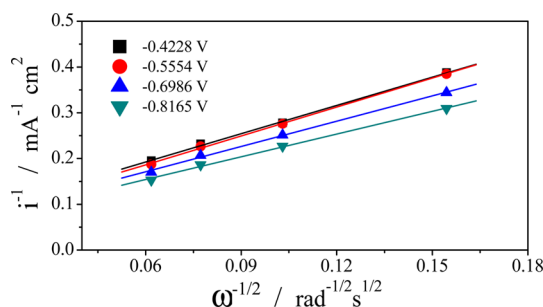
Figure 6. K−L plots at selected potentials.

Figure 4 are shown in Figure 6, respectively, by using the following equations:[4,42]

$$\frac{1}{i_d} = \frac{1}{i_k} + \frac{1}{i_{dl}} \tag{3}$$

$$i_k = nFAkC_{O_2} \tag{4}$$

$$i_{dl} = 0.62nFC_{O_2}D_{O_2}^{2/3}\nu^{-1/6}\omega^{1/2} = B\omega^{1/2} \tag{5}$$

$$\frac{1}{i_d} = \frac{1}{i_k} + \frac{1}{i_{dl}} = \frac{1}{i_k} + \frac{1}{B}\omega^{-1/2} \tag{6}$$

where i_d, i_k, and i_{dl} are the tested disk current density, kinetic current density, and film diffusion-limiting current density, respectively. Furthermore, n is the number of electrons in the ORR, F is the Faraday constant (96500 C mol^{-1}), A is the area of the disk electrode (0.196 cm^{-2}), C_{O_2} is the oxygen concentration in 0.1 M KOH (1.14×10^{-6} mol cm^{-3}), D_{O_2} is the oxygen diffusion coefficient in 0.1 M KOH (1.73×10^{-5} cm^2 s^{-1}), ν is the kinematic viscosity of the 0.1 M KOH solution (0.01 cm^2 s^{-1}), ω is the electrode rotation rate (rpm), and k is the rate constant for the ORR. There should be a linear relationship between i_d^{-1} and $\omega^{-1/2}$, the intercept is equal to i_k^{-1}, and the number of electrons transferred during the reaction could be calculated from the slope.

Symbols in Figure 6 represent experimental data, and straight dashed lines are linear fitting results. All plots in Figure 6 demonstrate the linear and approximate parallel relationships with the $n = 4$ theoretical plot at selected applied potentials. Both of the experimental results suggest that the four-electron process is the dominating pathway for the ORR on the as-prepared Au-GDC nanotube catalyst, which will benefit the construction of fuel cells and metal air batteries with high efficiency.

The promising ORR activities of the as-prepared Au-GDC nanotube catalyst can be rationalized to several possible reasons. First, the high Au loading (0.1031 mg cm^{-2} calculated by TEM−EDX measurement) in the nanotube promotes efficient interfacial charge transfer during the ORR.[12,43] Also, the small size and high dispersity of the Au nanoparticles benefit O$_2$ activation. The decreased coordination of Au together with the reduced electrophilicty of the small nanoparticle gives rise to a corresponding decrease in the activation energy of the dissociative chemisorption of oxygen molecules, which further facilitates the four-electron reduction of O$_2$.[10,44,45] Further, XPS results indicate a strong interaction between the Au nanoparticles and the GDC nanotube. The combination of the Au nanoparticles and the GDC nanotube provides a synergetic coupling effect for enhancing the ORR activity.[46,47] GDC in the Au-GDC nanotube catalyst may not only serve as a support but also play a key role in transferring oxygen ions due to the high oxygen storage capacity and high oxygen ionic conductivity of GDC.

Finally, the durability of the Au-GDC nanotube catalyst and commercial Pt/C during the ORR is evaluated via the chronoamperometric method at −0.8 V (vs Ag/AgCl) in an O$_2$-saturated 0.1 M KOH solution at 2500 rpm, as shown in Figure 7. Impressively, the current density at the Au-GDC
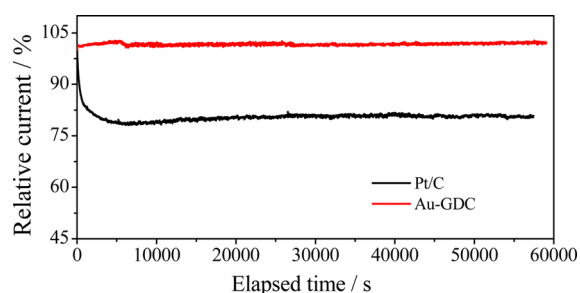
Figure 7. Current−time (i−t) chronoamperometric responses for the ORR at the as-prepared Au-GDC nanotubes and the commercial Pt/C catalyst in an O$_2$-saturated 0.1 M KOH solution at −0.8 V (vs Ag/AgCl) at 2500 rpm.

nanotube catalyst is very stable at the whole tested time (about 60000 s), and no current density decay has been observed, while a rapid 22% loss of the current density occurs for the commercial Pt/C catalyst in the initial 5000 s operation. This result exemplifies that the Au-GDC nanotube catalyst is more stable than the commercial Pt/C catalyst. The better stability should be attributed to the unique structural design of the Au-GDC nanotube catalyst. In the catalyst, Au nanoparticles were decorated in the inner wall of the GDC nanotube; such a structural design can stabilize the Au nanoparticles against aggregation during the ORR process because of the maximum interaction between the Au nanoparticles and the GDC support. The TEM study after the durability test also indicates that the Au nanoparticles are stable without noticeable size change and aggregation, as shown in Figure S5 in the SI.

4. CONCLUSION

In summary, we have demonstrated a facile method to prepare Au-GDC nanotubes; in this unique structure, Au nanoparticles were uniformly decorated in the inner wall of the GDC nanotubes with high Au loading. Compared with GDC nanoparticles and the as-reported Au/rGO hybrid catalyst, an enhanced catalytic activity for the ORR has been obtained with the as-prepared Au-GDC nanotube catalyst. Most importantly, the as-prepared Au-GDC nanotube catalyst exhibits excellent stability for the ORR because of the maximum interaction between Au nanoparticles and the GDC support.

■ ASSOCIATED CONTENT

⑤ Supporting Information

TEM images of the Gd$_{0.3}$Ce$_{0.7}$(OH)CO$_3$ precursor and Gd$_{0.3}$Ce$_{0.7}$(OH)CO$_3$−GDC core−shell structure, CV curves of Au-GDC nanotube catalysts in N$_2$- and O$_2$-saturated KOH solutions, and TEM images of Au-GDC nanotube catalysts after the durability test. This material is available free of charge via the Internet at http://pubs.acs.org.

■ AUTHOR INFORMATION

Corresponding Author
*Tel: +86-51265221519. E-mail: yangrz@suda.edu.cn.

Notes
The authors declare no competing financial interest.

■ ACKNOWLEDGMENTS

■ REFERENCES

(1) Winter, M.; Brodd, R. J. *Chem. Rev.* **2004**, *104* (10), 4245−4270.
(2) Bruce, P. G.; Hardwick, L. J.; Abraham, K. M. *Mater. Res. Soc.* **2011**, *36*, 506−512.
(3) Debe, M. K. *Nature* **2012**, *486* (7401), 43−51.
(4) Liang, Y. Y.; Li, Y. G.; Wang, H. L.; Zhou, J. G.; Wang, J.; Regier, T.; Dai, H. J. *Nat. Mater.* **2011**, *10* (10), 780−786.
(5) Wang, W.; Wang, R. F.; Ji, S.; Feng, H. Q.; Wang, H. *J. Power Sources* **2010**, *195* (11), 3498−3503.
(6) Gasteiger, H. A.; Kocha, S. S.; Sompalli, B.; Wagner, F. T. *Appl. Catal., B* **2005**, *56* (1−2 SPEC. ISS.), 9−35.

(7) Wang, H.; Wang, R. F.; Li, H.; Wang, Q. F.; Kang, J.; Lei, Z. Q. *Int. J. Hydrogen Energy* **2011**, *36* (5), 839−848.

(8) Kannan, P. Thesis for the degree of Doctor of Philosophy, 2011, p 67.

(9) Nøskov, J. K.; Rossmeisl, J.; Logadottir, A.; Lindqvist, L.; Kitchin, J. R.; Bligaard, T.; Jónsson, H. *J. Phys. Chem. B* **2004**, *108* (46), 17886−17892.

(10) Jeyabharathi, C.; Kumar, S. S.; Kiruthika, G. V. M.; Phani, K. L. N. *Angew. Chem., Int. Ed.* **2010**, *49* (17), 2988−3005.

(11) Chen, W.; Chen, S. *Angew. Chem., Int. Ed.* **2009**, *48* (24), 4386−4389.

(12) Lee, Y.; Loew, A.; Sun, S. *Chem. Mater.* **2010**, *22* (3), 755−761.

(13) Schmid, G.; Chi, L. F. *Adv. Mater.* **1998**, *10* (7), 515−526.

(14) Häkkinen, H. *Chem. Soc. Rev.* **2008**, *37* (9), 1847−1859.

(15) Wang, Y. J.; Wilkinson, D. P.; Zhang, J. *Chem. Rev.* **2011**, *111* (12), 7625−7651.

(16) Yin, H. J.; Tang, H. J.; Wang, D.; Gao, Y.; Tang, Z. Y. *ACS Nano* **2012**, *6* (9), 8288−8297.

(17) Nitani, H.; Nakagawa, T.; Daimon, H.; Kurobe, Y.; Ono, T.; Honda, Y.; Koizumi, A.; Seino, S.; Yamamoto, T. A. *Appl. Catal., A* **2007**, *326* (2), 194−201.

(18) Wang, X. L.; Zhang, H. M.; Zhang, J. L.; Xu, H. F.; Zhu, X. B.; Chen, J.; Yi, B. L. *J. Power Sources* **2006**, *162* (1), 474−479.

(19) Castellani, N. J.; Branda, M. M.; Neyman, K. M.; Illas, F. *J. Phys. Chem. C* **2009**, *113* (12), 4948−4954.

(20) Hornés, A.; Hungría, A. B.; Bera, P.; Cámara, A. L. p.; Fernández-García, M.; Martínez-Arias, A.; Rodriguez, J. A. *J. Am. Chem. Soc.* **2010**, *132* (1), 34−35.

(21) Han, M. M.; Wang, X. J.; Shen, Y. N.; Tang, C. H.; Li, G. S.; Smith, R. L. *J. Phys. Chem. C* **2010**, *114* (3), 793−798.

(22) Kydd, R.; Scott, J.; Teoh, W. Y.; Chiang, K.; Amal, R. *Langmuir* **2010**, *26* (3), 2099−2106.

(23) Chu, Y. Y.; Wang, Z. B.; Jiang, Z. Z.; Gu, D. M.; Yin, G. P. *Adv. Mater.* **2011**, *23* (24), 3100−3104.

(24) Yu, T.; Zeng, J.; Lim, B.; Xia, Y. N. *Adv. Mater.* **2010**, *22* (45), 5188−5192.

(25) Wang, J. S.; Xi, J. Y.; Bai, Y. X.; Shen, Y.; Sun, J.; Chen, L. Q.; Zhu, W. T.; Qiu, X. P. *J. Power Sources* **2007**, *164* (2), 555−560.

(26) Carrettin, S.; Conee Peion, P.; Corma, A.; Nieto, J. M. L.; Puntes, V. F. *Angew. Chem., Int. Ed.* **2004**, *43* (19), 2538−2540.

(27) Ji, X.; Evers, S.; Lee, K. T.; Nazar, L. F. *Chem. Commun.* **2010**, *46* (10), 1658−1660.

(28) Lou, X. W.; Archer, L. A.; Yang, Z. C. *Adv. Mater.* **2008**, *20* (21), 3987−4019.

(29) Zhang, D. F.; Sun, L. D.; Jia, C. J.; Yan, Z. G.; You, L. P.; Yan, C. H. *J. Am. Chem. Soc.* **2005**, *127* (39), 13492−13493.

(30) Zhou, K.; Yang, Z.; Yang, S. *Chem. Mater.* **2007**, *19* (6), 1215−1217.

(31) Zeng, H. C. *J. Mater. Chem.* **2006**, *16* (7), 649−662.

(32) Xia, Y.; Tang, Z. *Adv. Funct. Mater.* **2012**, *22* (12), 2585−2593.

(33) Chen, G.; Sun, S.; Zhao, W.; Xu, S.; You, T. *J. Phys. Chem. C* **2008**, *112* (51), 20217−20221.

(34) Chen, G.; Sun, S.; Sun, X.; Fan, W.; You, T. *Inorg. Chem.* **2009**, *48* (4), 1334−1338.

(35) Jin, C.; Liu, J. *J. Alloys Compd.* **2009**, *474* (2), 573−577.

(36) Fu, C. J.; Chan, S. H.; Ge, X. M.; Liu, Q. L.; Pasciak, G. *Int. J. Hydrogen Energy* **2011**, *36* (21), 13727−13734.

(37) Jin, C.; Cao, X. C.; Zhang, L. Y.; Zhang, C.; Yang, R. Z. *J. Power Sources* **2013**, *241*, 225−230.

(38) Sunarso, J.; Torriero, A. A.; Zhou, W.; Howlett, P. C.; Forsyth, M. *J. Phys. Chem. C* **2012**, *116* (9), 5827−5834.

(39) He, C.; Kunz, H. R.; Fenton, J. M. *J. Electrochem. Soc.* **1997**, *144* (3), 970−979.

(40) Roche, I.; Chainet, E.; Chatenet, M.; Vondrak, J. *J. Phys. Chem. C* **2007**, *111* (3), 1434−1443.

(41) Hyodo, T.; Kayashi, M.; Miura, N.; Yamazoe, N. *J. Electrochem. Soc.* **1996**, *143* (11), L266−L267.

(42) Cheng, F. Y.; Su, Y.; Liang, J.; Tao, Z. L.; Chen, J. *Chem. Mater.* **2009**, *22* (3), 898−905.

(43) Chen, W.; Ny, D.; Chen, S. *J. Power Sources* **2010**, *195* (2), 412−418.

(44) Tang, W.; Lin, H.; Kleiman-Shwarsctein, A.; Stucky, G. D.; McFarland, E. W. *J. Phys. Chem. C* **2008**, *112* (28), 10515−10519.

(45) Pal, R.; Wang, L.; Pei, Y.; Wang, L.; Zeng, X. C. *J. Am. Chem. Soc.* **2012**, *134* (22), 9438−9445.

(46) Zhang, N.; Liu, S.; Xu, Y. J. *Nanoscale* **2012**, *4* (7), 2227−2238.

(47) Mitsudome, T.; Mikami, Y.; Matoba, M.; Mizugaki, T.; Jitsukawa, K.; Kaneda, K. *Angew. Chem., Int. Ed.* **2012**, *51* (1), 136−139.